Control Engineering Practice 63 (2017) 81–90

Contents lists available at ScienceDirect

Control Engineering Practice

journal homepage: www.elsevier.com/locate/conengprac

Control-oriented tools for the design and validation of the JT-60SA magnetic control system

N. Cruz[a], G. De Tommasi[b,d], M. Mattei[c,d], A. Mele[b,d,*], Y. Miyata[e], A. Pironti[b,d], T. Suzuki[e]

[a] Instituto de Plasmas e Fusão Nuclear, Instituto Superior Técnico, Universidade de Lisboa, 1049-001 Lisboa, Portugal
[b] Dipartimento di Ingegneria Elettrica e delle Tecnologie dell'Informazione, Università degli Studi di Napoli Federico II, via Claudio 21, 80125 Napoli, Italy
[c] Dipartimento di Ingegneria Industriale e dell'Informazione, Seconda Università degli Studi di Napoli, via Roma 29, Aversa (CE) 80131, Italy
[d] Consorzio CREATE, via Claudio 21, 80125 Napoli, Italy
[e] National Institutes for Quantum and Radiological Science and Technology, Naka, Ibaraki 311-0193, Japan

ARTICLE INFO

Keywords:
JT-60SA
Control in fusion devices
Plasma magnetic control in tokamak

ABSTRACT

The construction and operation of the JT-60SA tokamak is the main project currently carried out jointly by Japan and the European Union under the Broader Approach agreement. Within the Integrated Project Team, Japanese and European scientists are developing and testing a number of tools to support preliminary studies and future operations of JT-60SA. Within this collaborative framework, European scientists are using a set of assessed modeling tools to design and validate possible solutions for the plasma magnetic control system of JT-60SA.

This paper introduces these tools and describes a possible control architecture to be used on the JT-60SA tokamak. The effectiveness of the proposed architecture is shown by means of numerical simulations.

1. Introduction

The Broader Approach (BA) is an agreement between the European Union and Japan that complements the ITER Project. BA aims to accelerate the realization of fusion energy by carrying out R & D, and by developing some advanced technologies for future demonstration fusion power reactors (Tsunematsu, 2009).

The Satellite Tokamak Programme (STP) is the main project within the BA umbrella; it includes the construction of the JT-60SA superconductive tokamak and its exploitation as an ITER "satellite" facility (Shirai, Barabarschi, & Kamada, 2016; Spears, 2014). The STP is expected to develop operating scenarios and address key physics issues for an efficient start up of ITER and for providing a continuous support to ITER experimentation. Furthermore it is expected that the operation of JT-60SA will complement the one of ITER in all areas of fusion R & D which are necessary to proceed with the design and realization of DEMO (http://www.jt60sa.org/pdfs/JT- 60SA Res Plan.pdf).

The European contribution to the STP programme is significant and it is not limited to the tokamak construction. Indeed, European scientists are actively contributing to the definition of the JT-60SA research plan (Giruzzi et al., 2016), and it is planned that the European team will be actively involved in the operations, playing a relevant role. For this reason, preliminary studies related to the exploitation of JT-60SA are currently carried out in different fields by European scientists in collaboration with Japanese colleagues.

Furthermore, the European Union aims at participating not only to the physics exploitation, but also at giving engineering support during the operations (Giruzzi et al., 2016; Innocente et al., 2015).

In this context the European fusion community is developing a number of tools for the design and validation of control systems, especially for magnetic axisymmetric control (Ariola & Pironti, 2016; De Tommasi et al., 2011).

Axisymmetric magnetic control deals with the control of the external magnetic field in a tokamak, which is necessary to achieve and maintain the desired *operational scenario*, that includes the desired current, and the desired shape and position of the plasma column within the vacuum chamber. On top of that, in all modern high performance tokamaks, due to elongated plasmas, magnetic control is also mandatory in order to vertically stabilize the plasma column. Moreover, for energetic reasons, the plasma should occupy as much volume as possible; this means that the distance between the plasma boundary and the facing metallic structures should be kept small and should be robustly controlled. To sum up, magnetic control represents the basic feedback control system that is needed in a tokamak since early operation phases, including the commissioning of the power supplies for the Poloidal Field (PF) coils, since magnetic control usually

* Corresponding author at: Dipartimento di Ingegneria Elettrica e delle Tecnologie dell'Informazione, Università degli Studi di Napoli Federico II, via Claudio 21, 80125 Napoli, Italy.
E-mail addresses: nunocruz@lei.fis.uc.pt (N. Cruz), detommas@unina.it (G. De Tommasi), massimiliano.mattei@unina2.it (M. Mattei), adriano.mele@unina.it (A. Mele), miyata.yoshiaki@qst.go.jp (Y. Miyata), pironti@unina.it (A. Pironti), suzuki.takahiro@qst.go.jp (T. Suzuki).

http://dx.doi.org/10.1016/j.conengprac.2017.03.009
Received 14 October 2016; Received in revised form 20 January 2017; Accepted 22 March 2017

includes also the regulation of the current in the PF circuits (Sartori, De Tommasi, & Piccolo, 2006; Yuan et al., 2013).

Within the European fusion community, the CREATE team has gained a significant experience in developing tools for the design and validation of magnetic control systems. The tools developed by CREATE have been validated on a number of different experimental devices (among the various see Albanese, Mattei, & Villone, 2004; Chen et al., 2016; Villone, Vyas, Lister, & Albanese, 1997), and have been successfully used to design magnetic control systems, for example at TCV (Ariola, Ambrosino, Pironti, Lister, & Vyas, 2002) and JET (Ambrosino, Ariola, Pironti, & Sartori, 2008; De Tommasi et al., 2012, 2014b; Marchiori et al., 2016). Furthermore, these tools are currently used to propose an enhancement of the EAST plasma control system (Albanese et al., 2016), and to perform preliminary studies and code benchmarking for both ITER (Ambrosino et al., 2015; Neto et al., 2015; Zabeo et al., 2014) and DEMO (Wenninger et al., 2015).

Within the dedicated workpackage of the Eurofusion activities, the CREATE tools are currently exploited to perform preliminary studies on the plasma magnetic control of JT-60SA. In particular, this paper reports on a possible architecture for this control system that has been designed and validated in simulation by exploiting the CREATE modeling codes.

It should be noticed that the equilibrium codes presented in this paper can be effectively used also to benchmark the scenarios studies made by the Japanese scientists (Miyata, Suzuki, Ide, & Urano, 2014); an example of comparison between equilibria is given in this paper.

The paper is structured as follows: Section 2 gives a description of the JT-60SA PF coils system and introduces to the main axisymmetric magnetic control problems. Section 3 describes the tools that have been developed to design and validate magnetic control systems. A possible architecture for the magnetic control system of JT-60SA is proposed in Section 4, while some preliminary simulation results obtained using the proposed tools are presented in Section 5. Eventually, some conclusive remarks are given.

2. Magnetic control in JT-60SA

In this section, first a brief description of the main characteristics of the JT-60SA tokamak and, in particular, of its PF coils is given; these coils, indeed, represent the actuators used by any magnetic control system. In the second part, the reader is introduced to the main axisymmetric magnetic control problems, i.e. plasma current, position and shape control.

2.1. The JT-60SA PF coils system

The JT-60SA tokamak is currently under construction in Naka, in the Ibaraki Prefecture of Japan, as a part of STP. The plasma in the JT-60SA vacuum chamber will have a major radius of 2.96 m and a minor radius of 1.18 m, with an overall plasma volume of 132 m^3 (Spears, 2014). The maximum plasma current envisaged for JT-60SA is 5.5 MA for a plasma with a relatively low aspect ratio (elongation $\kappa = 1.93$ and triangularity $\delta = 0.53$), and 4.6 MA for an *ITER-shaped* plasma ($\kappa = 1.8$ and $\delta = 0.43$). The maximum pulse duration will be about 100 s (http://www.jt60sa.org/pdfs/JT- 60SA Res Plan.pdf).

After the machine upgrade, JT-60SA will have a PF coils system consisting of two sets of superconductive coils: the Equilibrium Field Coils (*EF*1–6) made of Niobium–Titanium (NbTi), and the Central Solenoid (consisting of four independent coils, named *CS*1–4) in Niobium–Tin (Nb_3Sn). Furthermore, two *in-vessel* Fast Plasma Position copper Coils (*FPPC*1–2) will also be installed. Fig. 1 shows the PF coils layout of JT-60SA.

As it will be shown later, the PF coils represent the actuators used by the magnetic control system; for the sake of completeness, it is worth to mention that there exist in literature proposals to exploit the PF coils also for other control tasks (see the example in Pajares & Schuster, 2016 the authors propose to use the in-vessel coils for burn control).

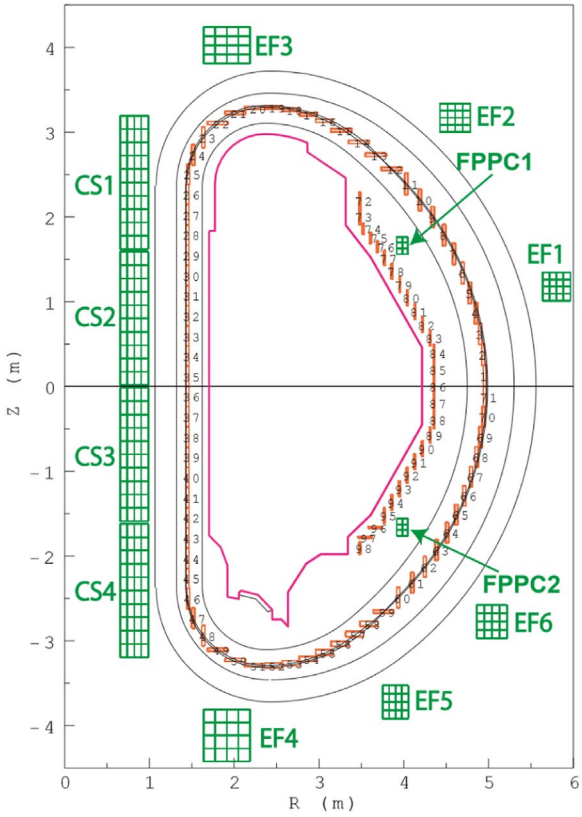

Fig. 1. JT-60SA poloidal cross-section and layout of the Poloidal Field coils system.

2.2. Axisymmetric control problems in tokamak

Plasma control is one of the crucial issues to be addressed in order to achieve the high performances in tokamak operations. In particular, magnetic axisymmetric control is an essential feature to achieve and maintain the desired *operational scenario*, and is needed since the very early plasma operation, including part of the integrated commissioning.

The magnetic control problem can be conceptually separated into three principal aspects (Ariola & Pironti, 2016):

- Position control.
- Plasma current control.
- Shape control.

Position control mainly deals with the control of the plasma vertical instabilities which affect elongated plasma configurations. The task of plasma vertical stabilization is usually carried out by exploiting the in-vessel coils, which are able to guarantee a faster response due to the fact that the electromagnetic field generated does not have to penetrate the metallic vessel structures. Such coils are placed inside the vessel, as near as possible to the plasma, in order to react fast and stabilize the plasma. Being installed inside the vessel, these are copper coils, since it would be impossible to keep superconductive in-vessel at the requested temperatures.

In order to make the design of the other controllers straightforward and to achieve better performances, it is a good practice to design this controller with a relatively large frequency bandwidth, which translates into a fast response and a decoupling from the other control actions (De Tommasi et al., 2011, Section 3).

Plasma current control takes care of regulating the plasma current

to the desired value; usually, this is done mainly (but not only) exploiting the central solenoid. The plasma, from this point of view, can be seen as the secondary coil of a transformer. Usually, it is desirable to have a plasma current control which is robust enough to work with different scenarios, independently of the desired plasma shape.

Finally, *Shape control* is responsible for the plasma to achieve a desired shape; this goal is reached by regulating the position of some points along the plasma boundary (reconstructed by a proper real-time estimation code).

It is worth to remark that, although not strictly included into the axisymmetric control problems, the regulation of the currents into the PF coils is usually included in the magnetic control system.

Indeed, plasma scenarios are defined in terms of nominal currents into the PF coils. Furthermore, the other control loops described so far can be designed in such a way to compute additional references for the PF current control. It turns out that a reliable *PF current control system* is needed, in order to track the desired references.

3. Tools for design and validation of magnetic control

In order to design and validate the proposed architecture for the JT-60SA magnetic control system described in Section 4, a set of Matlab/Simulink® tools has been set up.

Such tools exploit linearized plasma models generated by means of the CREATE equilibrium codes. These models are integrated into a Simulink scheme which reproduces the behaviour of the magnetic control system; the simulation scheme is initialized by means of a dedicated Matlab procedure. A similar approach has already been adopted in order to reproduce the experimental behavior of different fusion experimental devices, such as JET (De Tommasi et al., 2007, 2012), and more recently the EAST tokamak (Albanese et al., 2016). The availability of two different equilibrium codes, namely CREATE-L (Albanese & Villone, 1998) and CREATE-NL (Albanese, Ambrosino, & Mattei, 2015) is exploited for code benchmarking (see Section 3.1).

The same modelling tools are currently used not only for the design of JT-60SA, but also to perform preliminary studies and code benchmarking for both ITER (Neto et al., 2015) and DEMO (Wenninger et al., 2015).

Both the CREATE-L and CREATE-NL equilibrium codes automatically generate linearized models which can be used to design and validate magnetic control architectures. The main differences between these two codes consist in the adopted finite-element order scheme (first order for CREATE-NL and second order for CREATE-L), and in the Jacobian matrix calculation method for the implementation of the Newton method solver (analytic for CREATE-L, and numeric for CREATE-NL). Furthermore, CREATE-NL can be also used to validate control systems by means of nonlinear dynamic simulations, and has been also coupled with transport codes for integrated simulations (Romanelli et al., 2014).

Regardless of the specific equilibrium code used to derive it, the linearized model is given as state-space model:

$$\delta\dot{\mathbf{x}}(t) = \mathbf{A}\delta\mathbf{x}(t) + \mathbf{B}\delta\mathbf{u}(t) + \mathbf{E}\delta\dot{\mathbf{w}}(t), \tag{1a}$$

$$\delta\mathbf{y}(t) = \mathbf{C}\delta\mathbf{x}(t) + \mathbf{F}\delta\mathbf{w}(t), \tag{1b}$$

where:

- $\mathbf{A}$, $\mathbf{B}$, $\mathbf{E}$, $\mathbf{C}$ and $\mathbf{F}$ are the model matrices;
- $\delta\mathbf{x}(t) = (\delta\mathbf{I}_{PF}^{\mathrm{T}}(t)\delta\mathbf{I}_{eddy}^{\mathrm{T}}(t)\delta I_p(t))^{\mathrm{T}} \in \mathbb{R}^{(n_{PF}+n_e+1)}$ is the state space vector, which includes the n_{PF} variations of the currents in the PF circuits, of the eddy currents in the n_e circuits used to model the passive structures, and the variation of the plasma current I_p;
- $\delta\mathbf{u}(t) = (\delta\mathbf{U}_{PF}^{\mathrm{T}}(t)\ \mathbf{0}\ U_p)^{\mathrm{T}} \in \mathbb{R}^{(n_{PF}+n_e+1)}$ are the input voltage variations that includes the control voltages applied to the PF circuits $\mathbf{U}_{PF}(t)$, and the opposite of the equilibrium plasma voltage, which is assumed constant and equal to $Up = -r_p I_{p_0}$, where r_p is the estimated plasma resistance, and I_{p_0} is the value of the plasma current at the equilibrium;
- $\delta\mathbf{w}(t) = \left(\delta\beta_p(t)\delta l_i(t)\right)^{\mathrm{T}} \in \mathbb{R}^2$ are the variations of the poloidal beta β_P and of the internal disturbance l_i, which act as disturbances from the magnetic control point of view;
- $\delta\mathbf{y}(t) \in \mathbb{R}^{n_y}$ is the output vector that includes all the variables that need to be controlled (e.g., $I_P(t)$ the fluxes in the control points for plasma boundary control, the currents in the PF circuits $\mathbf{I}_{PF}(t)$, etc.).

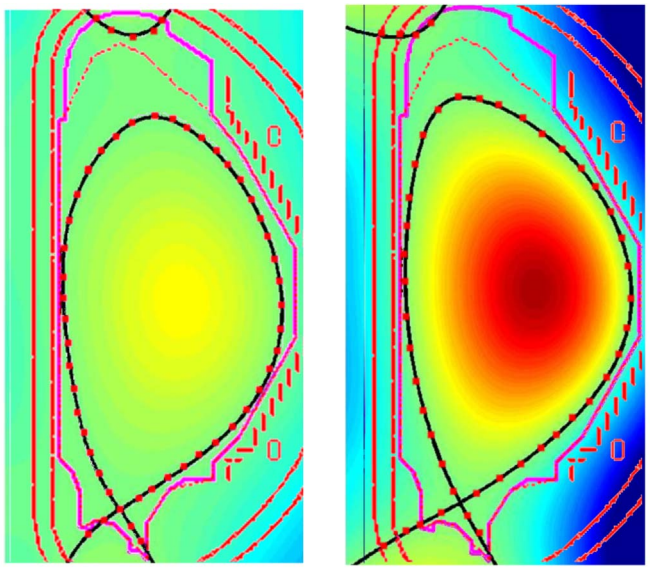

(a) Comparison for Scenario 2 at $t = 4.6$ s. (b) Comparison for Scenario 2 at $t = 18.6$ s.

Fig. 2. Comparison of the plasma shapes obtained with the TOSCA and CREATE-L equilibrium codes for two snapshots of the JT-60SA Scenario 2. The TOSCA plasma boundary is plot in solid black, while the CREATE-L boundary is plot in red dots. (For interpretation of the references to colour in this figure caption, the reader is referred to the web version of this paper.)

Given the adopted description for the passive structures of JT-60SA, the dimension of the state space for model (1) is equal to 140.

3.1. Benchmarking of plasma equilibria

As an example of code benchmarking, this section reports on the comparison between the plasma equilibria obtained with CREATE-L, and the ones obtained with TOSCA (Shinya, 2000), MECS (Miyata et al., 2014), and CarMa0 (Portone, Villone, Liu, Albanese, & Rubinacci, 2008 2008).

In particular, Fig. 2(a) and (b) shows a comparison between the shape obtained with TOSCA (left-hand side) and CREATE-L (right-hand side) for Scenario 2 at t=4.6 s and t=18.6 s, respectively. Scenario 2 is single null and full inductive (the definition of the JT-60SA scenarios can be found in JT-60SA Team (2015, Section 1.2).

Moreover, Table 1 reports a comparison of the growth rates obtained with CREATE-L, CarMa0 and MECS[1] for two snapshots of the Scenario 2. The computation of the growth rate has been performed taking into account both the active coils and the passive structure, i.e. it has been assumed that the PF coils will be controlled in a *voltage-driven* mode, coherently with the proposed control architecture. Furthermore, taking into account that CarMa0 is a 3D electromagnetic linear simulation code of the conductive coils and passive structures

[1] While TOSCA is the tool used by the JT-60SA home team to define the scenarios, MECS is used by the same team to estimate the growth rate.

Table 1
Comparison of the growth rate γ for two snapshots of JT-60SA Scenario 2.

Equilibrium code	t = 4.6 s, I_p = 1.4 MA, l_i=0.85, β_p = 0.21	t=18.6 s, I_p = 5.5 MA, l_i=0.85, β_p = 0.53
CREATE-L	8.35 s^{-1}	3.89 s^{-1}
CarMa0 2D mesh	8.32 s^{-1}	4.31 s^{-1}
CarMa0 3D mesh	9.22 s^{-1}	4.68 s^{-1}
MECS	12.43 s^{-1}	4.65 s^{-1}

coupled with a CREATE-L-like axisymmetric plasma, it should be noticed that the 3D effects, which typically reduce the stabilization capability of the passive structures, do not have a major impact on the growth rate. We can conclude that the proposed 2D modelling tools are reliable for the design of magnetic control systems.

4. Proposal for the JT60-SA magnetic control architecture

In this section, a possible architecture for the JT-60SA magnetic control system is proposed and discussed. Its effectiveness is shown by means of simulations, as it is reported in Section 5.

The proposed magnetic control system architecture consists of:

- A Poloidal Field Coils Current Controller, which grants that the PF coils achieve the reference current requested from the outer control loops.
- A Vertical Stabilization Controller, which takes care of vertically stabilize the unstable plasma column. For the reasons exposed in Section 2, this controller exploits the FPPC coils.
- A Plasma Current Controller, which regulates the plasma current to a desired value. This controller mainly exploits the CS coils (together with EF1–6).
- A Shape Controller, which causes the plasma boundary to move in order to achieve a desired plasma shape. This controller makes use of both EF and CS coils.

A block diagram of the control architecture is shown in Fig. 3.

In the following, a detailed discussion of each of the control system listed above is given.

4.1. Vertical stabilization control

In order to vertically stabilize the plasma, two possible solutions have been explored and are presented in this section.

The first solution computes the voltage requests to the FPPC coils as a linear combination of the vertical velocity of the plasma and the FPPC *imbalance* current. Indeed, the two in-vessel coils are driven in anti-series, that is the current in the upper coil flows in the opposite way with respect to the one in the lower coil. Given this connections setup, the vertical stabilization system can consider the FPPC coils as a single circuit, where $I_{FPPC}(t)$ is the imbalance current between the two coils, and $U_{FPPC}(t)$ is the voltage to be applied, with opposite signs, to the coils.

It turns out that the voltage applied to the FPPC coils is calculated as:

$$U_{FPPC}(t) = k_1 I_{FPPC}(t) + k_2 \dot{z}_p(t). \tag{2}$$

By tuning in a proper way the weights of the linear combination in (2), it is possible to obtain zero velocity in the vertical direction while maintaining low imbalance current $I_{FPPC}(t)$ in the in-vessel coils (i.e. far from the saturation limits).

It is worth noticing that all the parameters of the controller can be kept constant when moving from one scenario to another; the only exception is the gain k_2, which scales with the inverse of the plasma current I_p.

The robustness of the proposed approach with respect to variations of the model parameters can be evaluated by means of classical single-input–single-output (SISO) tools, when the open-loop transfer function between $U_{FPPC}(t)$ and the linear combination $k_1 I_{FPPC}(t) + k_2 \dot{z}_p(t)$ is considered. As an example, the Nichols plots of the considered open-loop transfer functions obtained with linearized models of Scenario 1 at t=15.66 s,[2] and of Scenario 2 at t=0.06 s, t=0.16 s and t=18.66 s are shown in Fig. 4.[3] As it can be seen, the gain margin stays in the range [5.58, 9.83] dB, while the phase margin is in the interval [34.4, 65.0]°.

It is important to remark that the simple structure of the control law (2) with just two gains permits to foresee the realization of effective adaptive algorithms for the parameters tuning during real tokamak operations.

The second approach exploits a *near* optimal controller to achieve zero vertical position and velocity in a minimum time span. Given the system model, this method aims at simultaneously bringing the plasma to rest and to the reference position, by optimizing the time to target.

The method applied to improve the vertical stabilization system in TCV (Cruz, 2014; Cruz et al., 2015) was further developed using the CREATE plasma model. In Cruz et al. (2015) the method implemented for TCV Tokamak uses an extreme model reduction up to a second order model. Then this simplified model is used to build the controller. When applying the same model reduction to the JT-60SA tokamak and power supplies models, the accuracy of the reduced model was not enough to satisfy the representation of the complete model.

To solve this issue, we used a similar method to find the switch time and final time to target with the complete model, including the power supply, to design the controller. The time optimal control law algorithm using the complete model revealed to be too heavy for real-time implementation and would need the real-time input measurements of several states that are not expected to be available for control. The optimal state-space trajectory calculation needs information on the different states of the system, while the controller should only use the data from the output vector (plasma position and velocity).

To mitigate this difficulty the design of a near time optimal controller using plasma position and velocity was envisaged. The solution was to implement a proportional-integral-derivative (PID) controller with high gains tuned to approximate the behaviour of the bang-bang controller. The voltage applied to the FPPC coils is thus calculated as:

$$U_{FPPC}(t) = k_p z_p(t) + k_d \dot{z}_p(t). \tag{3}$$

where $U_{FPPC}(t)$ is the previously defined voltage to be applied, with opposite signs, to the coils, while k_p and k_d are the proportional and derivative gains of the controller, and $z_p(t)$ and $\dot{z}_p(t)$ are the plasma position and velocity respectively.

It should be noticed that, for both the proposed approaches, in order to minimize the effect of the noise on the z_p or $\dot{z}_p$ two different approaches can be adopted, depending on what measurement is provided by the magnetic diagnostic:

- if the position z_p is provided, then the minimization of the effect of the noise can be achieved by computing $\dot{z}_p$ via a derivative filter $s/(1 + s\tau_h)$, where τ_h is chosen according to the closed loop bandwidth of the vertical stabilization system (see the EAST case, Albanese et al., 2016);

[2] Scenario 1 is a full inductive double null plasma whose main parameters at t=15.66s are I_p=5.5MA, β_p = 0.53 and l_i=0.85.

[3] It is worth to recall that, as far as the magnetic control is concerned, the response described by the linear model (1) depends on the plasma parameters, i.e. the plasma shape, the plasma current I_p, and the internal profile descriptors β_p and l_i. Hence, a different snapshot during a given scenario returns different linearized models, with different values for the unstable mode and, more generally, with a different plasma response.

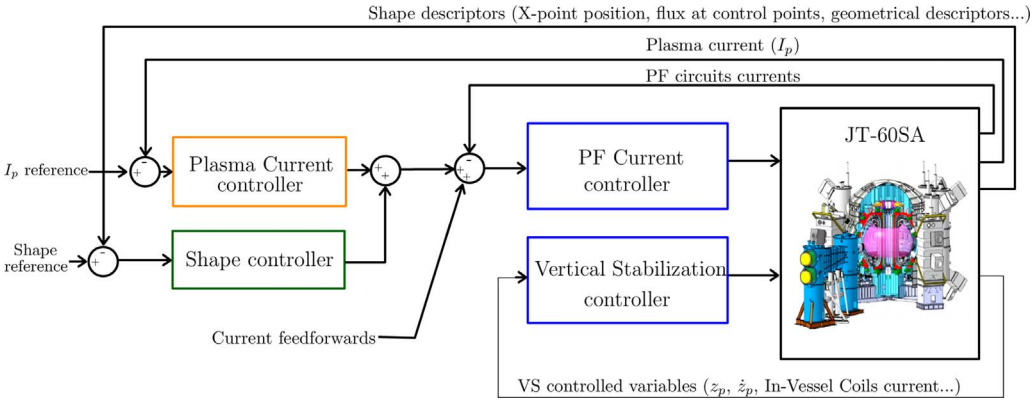

Fig. 3. Proposed architecture for the JT-60SA magnetic control system.

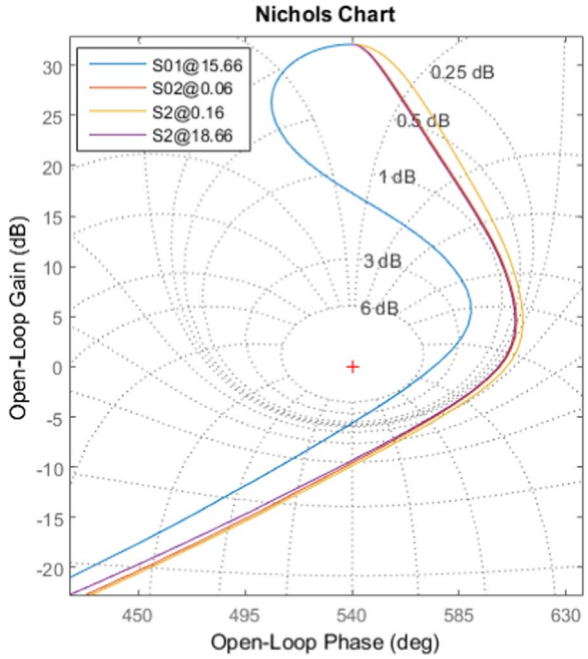

Fig. 4. Nichols plots for Scenarios 1 and 2.

- if the velocity is provided, then minimization of the noise can be achieved by oversampling the magnetic measurement (as an example, see the JET magnetic diagnostic, Batista, Sousa, & Varandas, 2006; De Tommasi et al., 2014a).

4.2. Plasma Current control

The Plasma Current control problem has been solved adopting a simple PID control logic. The current references for the CS and EF coils are calculated as

$$\mathbf{I}_{PF}(s) = \mathbf{K}_{p_{curr}}\left(k_P + \frac{k_I}{s} + k_D\frac{s\tau_D}{1+s\tau_D}\right)I_{p_e}(s), \tag{4}$$

where $I_{p_e}(s) = I_{p_{ref}}(s) - I_p(s)$ is the Laplace transform of the plasma current control error, while $\mathbf{K}_{p_{curr}}$ is a vector which contains a combination of the PF currents that causes a constant flux variation along a closed line containing the envisaged plasma boundary, that is the linear combination of the PF currents that provides the so-called *transformer field*. Such a combination of currents has been obtained via an optimization procedure, based on a model of the machine poloidal cross section (without plasma) obtained using a finite element method.

Similar to what has been seen for the vertical stabilization algorithm (2), the PID parameters in (4) can be tuned using SISO control design tools and the SISO open-loop transfer function between the considered linear combination of PF currents and I_P.

4.3. Shape control

The proposed Shape controller adopts an *Isoflux* control logic in order to achieve the desired plasma boundary for single null configurations: this approach aims at controlling the position of the X-point plus a set of flux differences between the flux at some control points chosen along the desired plasma boundary and the flux at the X-point itself. This purpose is obviously to be achieved by means of a proper control algorithm.

In the proposed control architecture, we adopted an approach similar to the one used for the eXtreme Shape Controller (XSC) at JET (Ambrosino et al., 2008), assuming that the PF current controller performs a perfect decoupling of the PF coils circuits (as discussed in Section 4.4). Under this hypothesis, each of the PF circuits can be treated as an independent SISO channels with a first order response; in particular, the time constants of the PF circuits can all be considered equal to τ_{PF}. This means that the i-th PF circuit can be modeled as:

$$I_{PF_i}(s) = \frac{I_{PF_{ref_i}}(s)}{1+s\tau_{PF}}, \tag{5}$$

where $I_{PF_i}(s)$ and $I_{PF_{ref_i}}(s)$ are the Laplace transforms of the i-th PF current measurement and reference, respectively.

The XSC then controls the whole plasma shape selecting the current into the PF coils on the base of the errors on the chosen control variables. Its design is based on the linear model output equation (1b), when only the output variables $\mathbf{y}_{sh}(t) \in \mathbb{R}^{n_{sh}}$ used to control the plasma shape are considered; hence:

$$\delta\mathbf{y}_{sh}(t) = \mathbf{C}_{sh}\,\delta\mathbf{I}_{PF}(t) + \mathbf{F}_{sh}\delta\mathbf{w}(t) \tag{6}$$

Given the isoflux approach considered in this paper, the output vector $\mathbf{y}_{sh}(t)$ includes the flux differences at the control points, and the position of the X-point. The choice of the control points is usually done, by selecting a sufficient number of segment to describe the plasma boundary. A technique for an optimal choice of the control segments is described in Pironti & Portone (1998), while a possible choice is shown in Fig. 5.

Let $\delta\mathbf{I}_{PF_N}(s)$ and $\delta\mathbf{Y}_{sh}(s)$ be the Laplace transform of the current variations in the PF coils and of the plasma shape descriptors, respectively, when neglecting the effect of the disturbances in (6), it is:

$$\delta\mathbf{Y}_{sh}(s) = \mathbf{C}_{sh}\delta\mathbf{I}_{PF_N}(s).$$

It follows that:

$$\delta\mathbf{Y}_{sh}(s) = \frac{\mathbf{C}_{sh}}{1+s\tau_{PF}}\cdot\delta\mathbf{I}_{PF_{ref}}(s), \tag{7}$$

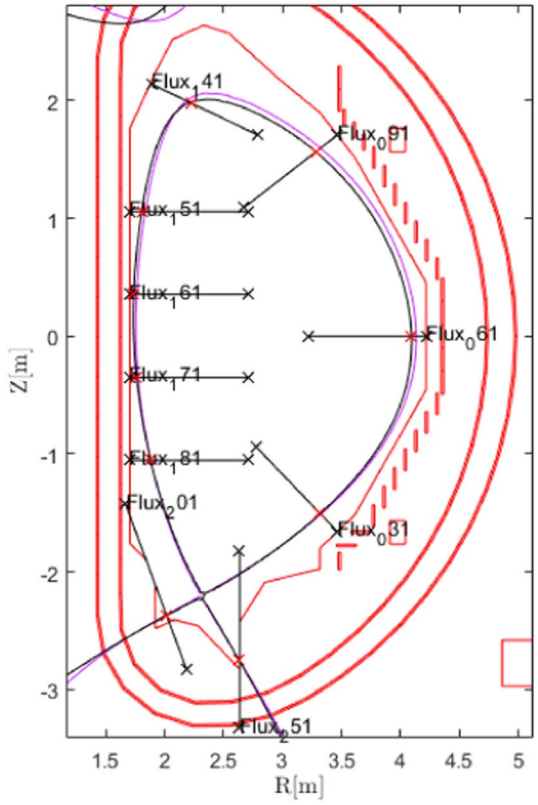

Fig. 5. Possible choice of the control segments used by the proposed isoflux approach for plasma shape control. This figure shows also the shape references for the simulation presented in Section 5.2. The initial shape is shown in magenta, while the target shape in reported black; the red markers represent the target points along the control segments. (For interpretation of the references to colour in this figure caption, the reader is referred to the web version of this paper.)

hence the plasma shape descriptors have the same dynamic response of the PF currents. Indeed, the effect of the eddy currents in the passive structure can be neglected when dealing with plasma shape and current control at JT-60SA, since the associated dynamics are faster than the one associated to the PF circuits (see also Ariola & Pironti, 2003 for more details).

Moreover, from (7) it follows that the design of the plasma shape controller can be based on the $\mathbf{C}_{sh}$ matrix following the *XSC-like* approach. The interested reader can refer to Ariola & Pironti (2005) for more details.

Here we just recall that, since usually $n_{PF} < n_{sh}$, at steady-state it is possible to control to zero the error on n_{PF} linear combinations of plasma shape descriptors. The choice the linear combinations to be controlled is carried out minimizing the following steady-state performance index:

$$J = \lim_{t \to +\infty} (\delta \mathbf{y}_{sh_{ref}} - \delta \mathbf{y}_{sh}(t))^T (\delta \mathbf{y}_{sh_{ref}} - \delta \mathbf{y}_{sh}(t)), \tag{8}$$

where $\delta \mathbf{y}_{sh_{ref}}$ are constant references to the controlled variables.

Minimization of (8) can be attained using the singular value decomposition (SVD) of the $\mathbf{C}_{sh}$ matrix. Furthermore, additional controllers can be included in the loop in order to achieve better performances during the transient. More details about how a dynamic plasma shape controller can be designed starting from the SVD of the $\mathbf{C}$ matrix can be found in Ariola & Pironti (2005).

Finally, it is worth noticing that such a control approach can be easily adapted to control different shape descriptors such as the distance between the plasma boundary and the first wall along some desired directions (as it is done at JET, Ambrosino et al., 2008). The variations of such geometrical descriptors of the plasma shape are already included among the outputs of the models generated by means of CREATE-L; nevertheless, an isoflux approach has been preferred, since it is the one currently envisaged by the JT-60SA research team. Furthermore, this approach can also be extended to double null configuration, which is one of the lines for further research.

4.4. PF current control

As it has been discussed in Section 2, the controllers described in the previous sections generate references for the PF coils currents. Hence, the magnetic control system has to rely on an effective PF coils current control algorithm. Furthermore, for the design of the shape controller it is required that the PF coils are decoupled and exhibit almost the same dynamic response (see Section 4.3).

The design of the proposed PF coils current control has been carried out starting from a plasmaless model of JT-60SA, following the steps described below:

- A modified version $\widetilde{\mathbf{L}}_{PF} \in \mathbb{R}^{n_{PF}} \times \mathbb{R}^{n_{PF}}$ of the inductance matrix of the PF circuits is calculated, by neglecting the effect of the passive structures. Furthermore, in order to minimize the control effort, in each row of the $\widetilde{\mathbf{L}}_{PF}$ matrix all the mutual inductance terms which are less than the 10% of the circuit self-inductance have been neglected. Indeed, in this way the current in each circuit is controlled only by the circuits that are more coupled with it, avoiding to easily saturate the voltages without gaining any practical improvement in the control of the PF currents.
- The time constants τ_{PF_i} for the response of the i-th circuit are chosen and used to construct a matrix $\Lambda \in \mathbb{R}^{n_{PF}} \times \mathbb{R}^{n_{PF}}$, defined as:

$$\mathbf{\Lambda} = \begin{pmatrix} 1/\tau_{PF1} & 0 & \dots & 0 \\ 0 & 1/\tau_{PF2} & \dots & 0 \\ \vdots & \vdots & \dots & \vdots \\ 0 & 0 & \dots & 1/\tau_{PF_n} \end{pmatrix}.$$

- The voltages to be applied to the PF circuits are then calculated as:

$$\mathbf{U}_{PF}(t) = \mathbf{K}_{PF} \cdot \left(I_{PF_{ref}}(t) - I_{PF}(t) \right),$$

where the control gain matrix $\mathbf{K}_{PF}$ is given by

$$\mathbf{K}_{PF} = \mathbf{S}^{-1} \cdot \widetilde{\mathbf{L}}_{PF} \cdot \mathbf{\Lambda},$$

and $\mathbf{S} \in \mathbb{R}^{n_{PF}} \times \mathbb{R}^{n_{PF}}$ is a diagonal polarity matrix that specifies the correct sign of the applied voltage for each circuit.

In the design of the PF current control, it has not been included any integral action, since the PF coils have been supposed to be perfectly superconductive (hence providing a "natural" integral action by themselves). In real operation, where this hypothesis may not be true, such a control action can be included easily; alternatively, if a good estimation of the coils resistance is available, the ohmic drop can be compensated via a feedforward action.

The bode diagrams of the closed loop PF coils current control system are reported in Fig. 6. It can be noticed how the diagonal channels (from the i-th voltage to the i-th current, Fig. 6(a)) exhibit very similar dynamic responses, while the off-diagonal channels (whose Bode diagrams are shown in Fig. 6(b)) have a much lower magnitude, hence proving that good decoupling is achieved.

5. Simulations

This section shows the performance of the proposed architecture and algorithms for the magnetic control of JT-60SA. First we show the behaviour of the vertical stabilization system when the maximum possible *Vertical Displacement Event* (VDE) is considered. In the second part of this section, some preliminary simulation results of the

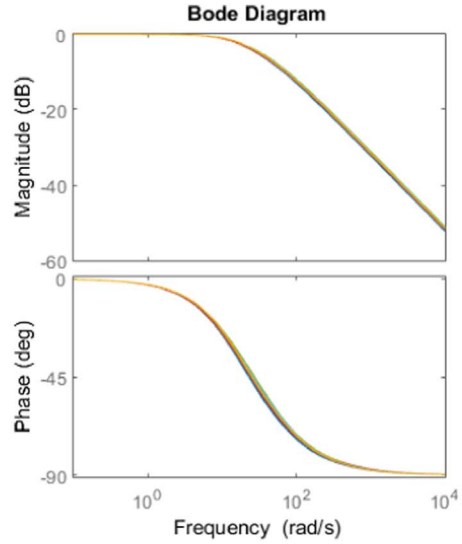

(a) Bode diagrams for the diagonal channels.

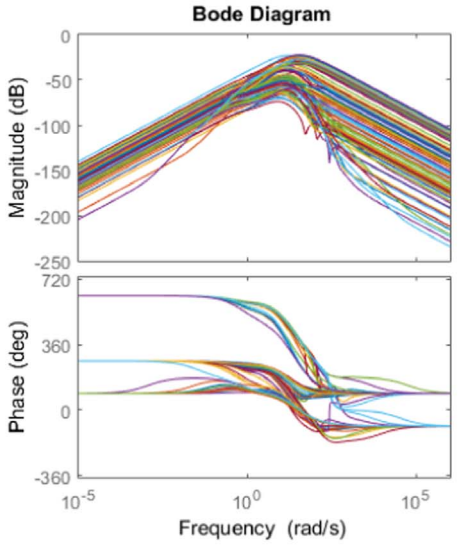

(b) Bode diagrams for the off-diagonal channels.

Fig. 6. Bode diagrams for the closed loop PF coils current control system.

overall magnetic control system are presented.

5.1. VDE rejection

In this section we study the performance of the near optimal vertical stabilization control system presented in Section 4.1 when rejecting a VDE. The presented results aim at evaluating the controller stability and performance, as well as assessing the controllability limits of the JT-60SA plant.

A VDE is an uncontrolled growth of the plasma unstable vertical mode. Although, the plasma is always vertically controlled, these uncontrolled growths can occur for different reasons, such as:

- fast disturbances acting on a time scale which is outside the control system bandwidth;
- delays in the control loop;
- wrong control action due to measurement noise, when plasma velocity is almost zero.

The behaviour of the near optimal vertical controller has been assessed using the linearized models of Scenarios 1 and 2. In

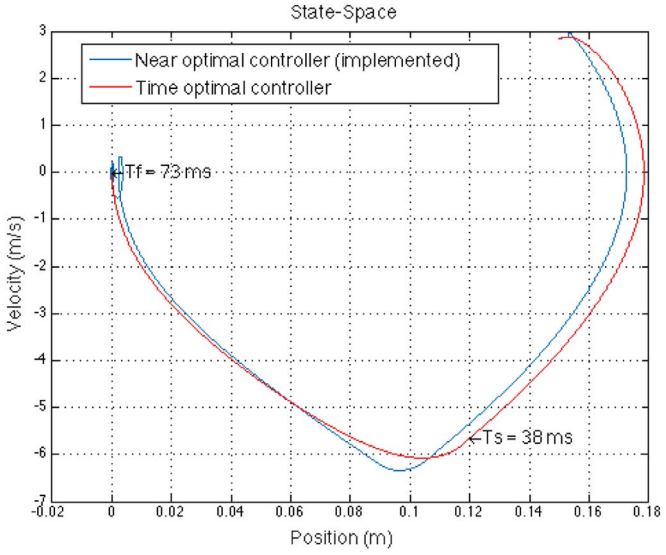

Fig. 7. Time optimal and near optimal trajectories for JT-60SA Scenario 1 with initial displacement of 15 cm.

particular, a VDE of 15 cm was considered, which, for these scenarios, represent the maximum displacement that can be accommodated before the plasma touches the first wall in the outer part of the vessel. Simulations have been carried out in order to estimate how the controller and plasma would behave under this limit situation. The initial plasma velocity is calculated by the combination of states that describe the currents in the passive structures of the vessel that are calculated for the given position.[4] This makes the initial velocity a realistic worst case situation when compared to the unrealistic case of simulating initial plasma velocity and currents in the vessel as zero. Furthermore, the power supplies for the in-vessel coils have been modelled as a first order low pass filter with a time constant $\tau_{PS} = 3$ ms, a pure delay of 1.5 ms, and capable to deliver a maximum voltage of 1 kV.

Figs. 7 and 8 present the projection of the state-space trajectory on the vertical position/vertical velocity plane when the same controller is used both for Scenarios 1 and 2. The figures depict the time optimal trajectory and the near optimal trajectory that was achieved using the implemented algorithm. The same control algorithm was tested under both scenarios to check the robustness under different conditions. As a result, it turned out that the control algorithm developed for Scenario 1 was robust enough to deal also with Scenario 2.

Fig. 9 reports the time evolution of plasma position and velocity, as well as the control signal for both the optimal and the near optimal controllers in Scenario 1 case. It should be noticed that, although the near time optimal control signal has some oscillations near the set point, the overall time performance is very close to the optimal controller. The time optimal controller of the system is a bang-bang controller with a single control switch. From this example it follows that by choosing the correct gains that saturate the actuators at the given voltage limit, a PID controller can replace the bang-bang controller achieving a similar behaviour. Moreover, note that the 15 cm VDE can be recovered in less than 100 ms.

For the sake of completeness, Fig. 10 shows a comparison between the behaviour of the near optimal controller and a vertical stabilization system implementing the control law (2), in the Scenario 2 case. The response of the latter is obviously slower (the VDE is recovered in about 150 ms), while the required control energy is less. Indeed, in the

[4] From the point of view of the vertical stabilization controller, a VDE is equivalent to a sudden and almost instantaneous change in plasma position, which causes an almost instantaneous change of the currents in model state $\mathbf{x}(t)$.

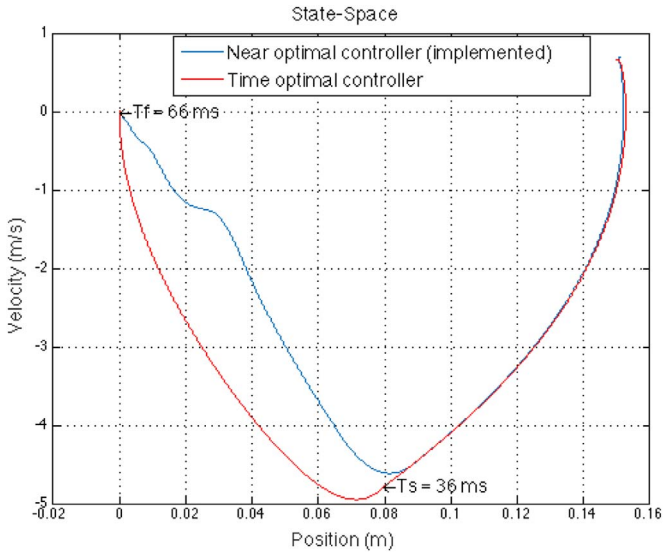

Fig. 8. Time optimal and near optimal trajectories for JT-60SA Scenario 2 with initial displacement of 15 cm.

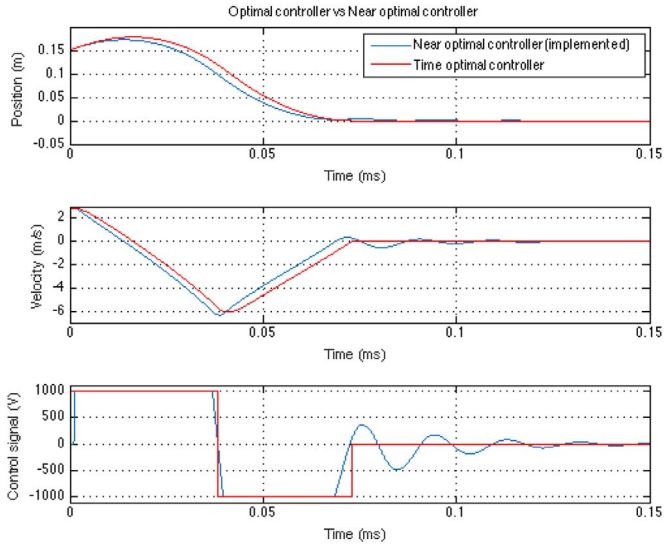

Fig. 9. VDE rejection. Time evolution for the optimal and near optimal trajectories when a 15 cm VDE is considered under JT-60SA Scenario 1.

Scenario 2 case the control energy is about 150 kJ for the near time optimal approach, while it is about 60 kJ when (2) is applied.

5.2. Simulations of the overall magnetic control system

In this section we show the performance of the overall magnetic control system described in Section 2 by means of simulations obtained using a linearized model of Scenario 2 at t=0.06 s, which corresponds to the equilibrium with I_p equal to 5.5 MA, β_p equal to 0.496, and l_i equal to 0.854.

A simplified model of the PF circuits power supplies has been included in the simulation scheme. Similar to what has been done for the in-vessel coils, each power supply has been modelled as a first order system with a 3 ms time constant, a pure delay of 1.5 ms, and a voltage saturation.

It is worth to notice that in the current version the CREATE linearized model provides all the reconstructed parameters as outputs.[5]

[5] All the quantities of interest for plasma magnetic control, i.e. the plasma current, the plasma shape and position, are reconstructed from the measurements delivered by the magnetic diagnostic system (De Tommasi, Neto, Pironti, & Sterle, 2015).

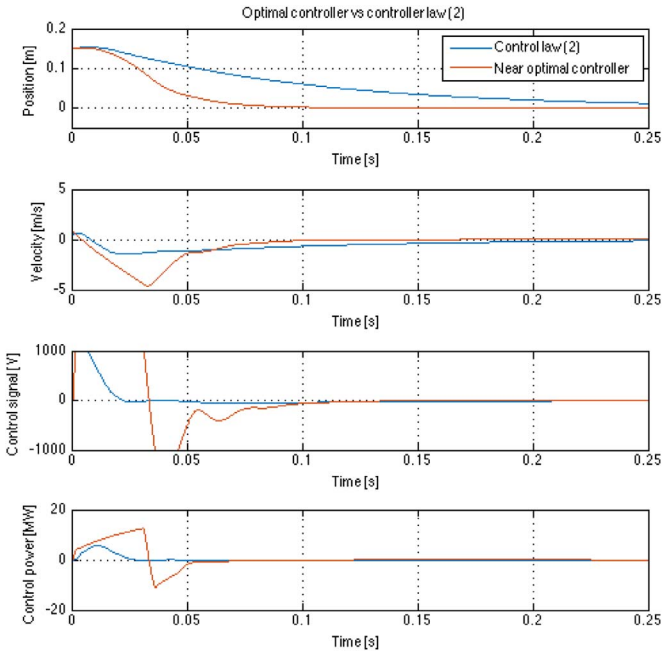

Fig. 10. VDE rejection. Comparison between the near optimal controller and the control (2) when a 15 cm VDE is considered under JT-60SA Scenario 2.

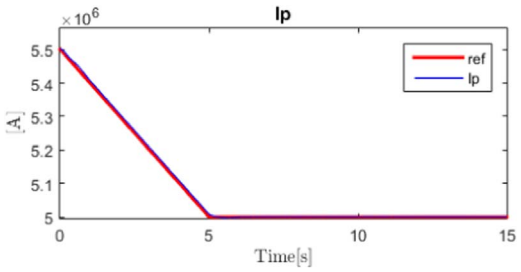

Fig. 11. Tracking of the plasma current for the simulation presented in Section 5.2.

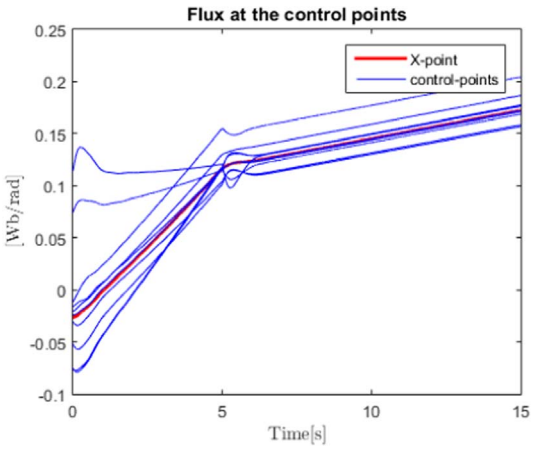

Fig. 12. Fluxes at the control point for the simulation presented in Section 5.2.

However, in future a block that models the plant magnetic diagnostic can be easily included in order to take into account the nonlinearities due to the reconstruction when validating the control algorithms (as it has been done in the case of the JET tokamak, see De Tommasi et al., 2007).

The results shown in Figs. 11–14 correspond to a variation of I_p of −0.5 MA in 5 s, plus a modification of the shape as shown in Fig. 5. In these figures, the references are reported in red, while the outputs of the simulation are in blue. For the magnetic fluxes at the shape control points (shown in Fig. 12), according to the *isoflux* control logic, the

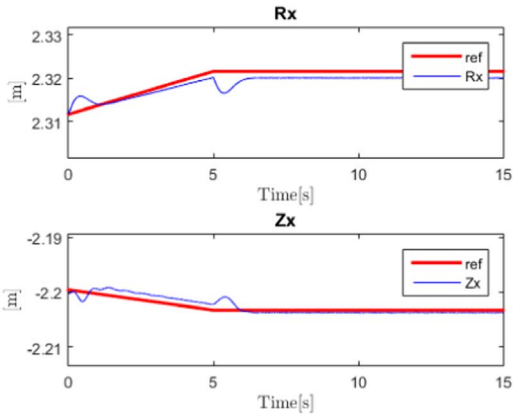

Fig. 13. Position of the X-point for the simulation presented in Section 5.2. The small bump at 5 s is due to the artificial waveforms assigned to poloidal beta and internal inductance.

power supplies (that includes also voltage and current saturations). In future, the modularity of the presented tools, which are based on Matlab/Simulink®, permits to easily include more detailed models of the plant (i.e., of the plasma/circuit model and/or the power supplies and/or the real-time plasma reconstruction code) in order to perform further validation of the control system.

It is worth to remark that, by exploiting the experience previously gained on a large number of fusion devices, the CREATE modeling tools have been easily customized for JT-60SA, allowing to design and validate an effective architecture for the complete magnetic control system.

The availability of engineering-oriented CREATE models can be exploited also to support the design and commissioning of the JT-60SA magnetic diagnostic (Peruzzo et al., 2009) and of the power supplies (Albanese et al., 2011). Furthermore, the CREATE-NL equilibrium code can be used to validate the control systems using nonlinear simulations of the whole pulse, from the breakdown to the end of the

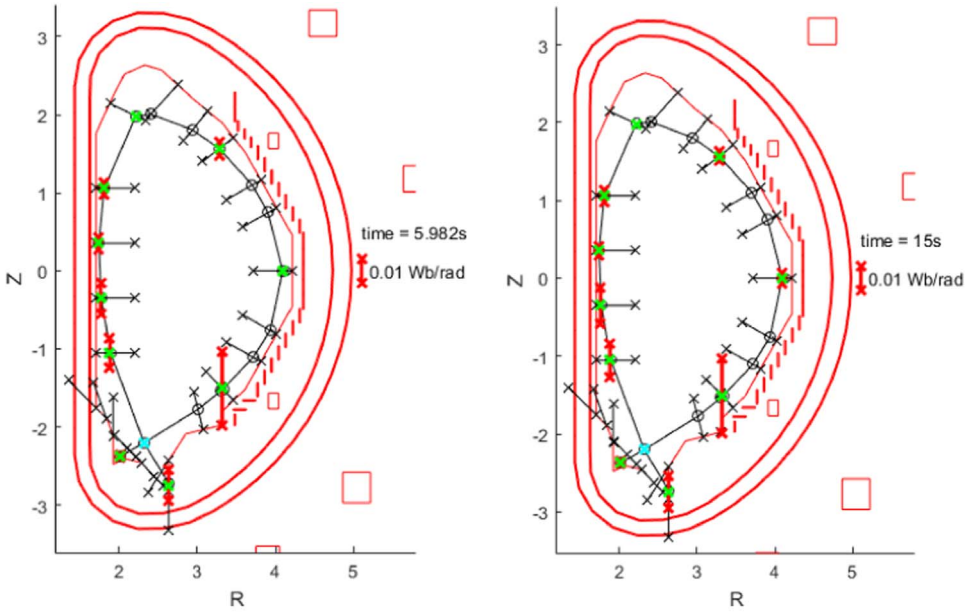

(a) Plasma shape at $t = 6$ s. (b) Plasma shape at $t = 15$ s

Fig. 14. Snapshots of the plasma poloidal cross section during the simulation presented in Section 5.2.

reference has been set equal to the simulated value of the flux at the null point, available among the outputs of the CREATE linearized models. The final shape is the one obtained generating a plasma equilibrium with CREATE-L for Scenario 2 at t=116.4 s[6]; this equilibrium has been used also to obtain the final values of β_{pol} and l_i; for the simulation purposes, the disturbances ramp from the initial to the final value during the transition time.

6. Conclusion

This paper reported on the European activities carried out for the design and validation of the JT-60SA magnetic control system. In particular a proposal for the overall architecture of the plasma magnetic control system has been presented, together with the algorithms to be implemented in each functional block. Validation of the proposed approach has been proved by means of simulations that exploit the CREATE plasma models and the simplified models of the plasma current ramp-down (Ambrosino et al., 2015). Furthermore, CREATE-NL can also be used to optimize and design advanced control algorithms for the breakdown phase (Albanese et al., 2013; Ambrosino, De Tommasi, Mattei, & Pironti, 2015).

[6] It is worth noticing that this time indication is meant to provide the reader with a reference to retrieve the information about the snapshot on the JT-60SA documentation. In what follows, all simulations have been assumed to start at $t = 0$ s for simplicity.

Acknowledgements

The authors gratefully acknowledge members of JT-60SA Integrated Project Team for data exchange and fruitful discussions. The authors would also like to thank Prof. Fabio Villone.

This work has been carried out within the framework of the EUROfusion Consortium and has received funding from the Euratom research and training programme 2014–2018 under grant agreement No 633053.

IST activities also received financial support from “Fundação para a Ciência e Tecnologia” through project UID/FIS/50010/2013.

The views and opinions expressed herein do not necessarily reflect those of the European Commission.

References

Albanese, R., Ambrosino, R., & Mattei, M. (2015). CREATE-NL+: A robust control-oriented free boundary dynamic plasma equilibrium solver. *Fusion Engineering and Design*, 96–97(October), 664–667.

Albanese, R., Ambrosino, G., Ariola, M., Artaserse, G., Bellizio, T., Coccorese, V. et al. (2011). Overview of modelling activities for Plasma Control Upgrade in JET. *Fusion Engineering and Design*, 86(October (6–8)), 1030–1033.

Albanese, R., Maviglia, F., Lomas, P. J., Manzanares, A., Mattei, M., Neto, A. et al. (2013). Experimental results with an optimized magnetic field configuration for JET breakdown. *Nuclear Fusion*, 52(December (12)), 123010.

Albanese, R., Ambrosino, R., Calabró, G., Castaldo, A., Crisanti, F., De Tommasi, G., et al. (2016). A MIMO architecture for integrated control of plasma shape and flux expansion for the EAST tokamak. In *Proceedings of the 2016 IEEE multi-conference on systems and control* (pp. 611–616), Buenos Aires, Argentina, September.

Albanese, R., Mattei, M., & Villone, F. (2004). Prediction of the growth rates of VDEs in JET. *Nuclear Fusion*, 44(September (9)), 999–1007.

Albanese, R., & Villone, F. (1998). The linearized CREATE-L plasma response model for the control of current, position and shape in tokamaks. *Nuclear Fusion*, 38(May (5)), 723–738.

Ambrosino, G., Ariola, M., Pironti, A., & Sartori, F. (2008). Design and implementation of an output regulation controller for the JET tokamak. *IEEE Transactions on Control Systems Technology*, 16(November (6)), 1101–1111.

Ambrosino, R., De Tommasi, G., Mattei, M., & Pironti, A. (2015). Model based optimization and estimation of the field map during the breakdown phase in the ITER tokamak. In *Proceedings of the 2015 IEEE multi-conference on systems and control* (pp. 1284–1289), Sydney, Australia, September.

Ambrosino, R., et al. (2015). Design and nonlinear validation of the ITER magnetic control system. In *Proceedings of the 2015 IEEE multi-conference on systems and control* (pp. 1290–1295), Sydney, Australia, September.

Ariola, M., Ambrosino, G., Pironti, A., Lister, J. B., & Vyas, P. (2002). Design and experimental testing of a robust multivariable controller on a tokamak. *IEEE Transactions on Control Systems Technology*, 10(September (5)), 646–653.

Ariola, M., & Pironti, A. (2003). An application of the singular perturbation decomposition to plasma position and shape control. *European Journal of Control*, 9(4), 433–443.

Ariola, M., & Pironti, A. (2005). The design of the eXtreme Shape Controller for the JET tokamak. *IEEE Control Systems Magazine*, 25(October (5)), 65–75.

Ariola, M., & Pironti, A. (2016). *Magnetic control of tokamak plasmas* (2nd ed.) London: Springer.

Batista, A. J. N., Sousa, J., & Varandas, C. A. F. (2006). ATCA digital controller hardware for vertical stabilization of plasmas in tokamaks. *Review of Scientific Instruments*, 77(October (10)), 10F527.

Chen, S. L., Villone, F., Xiao, B. J., Barbato, L., Mastrostefano, S., Luo, Z. P. et al. (2016). Equivalent axisymmetric plasma response models of EAST. *Plasma Physics and Controlled Fusion*, 58(February (2)) 025017-7.

Cruz, N. (2014). *Digital control system for vertical stability of the TCV plasma* (Ph.D. thesis).

Cruz, N., Moret, J.-M., Coda, S., Duval, B. P., Le, H. B., Rodrigues, A. P. et al. (2015). An optimal real-time controller for vertical plasma stabilization. *IEEE Transactions on Nuclear Science*, 62(December (6)), 3126–3133.

De Tommasi, G. et al. (2007). XSC Tools: A software suite for tokamak plasma shape control design and validation. *IEEE Transactions on Plasma Science*, 35(June (3)), 709–723.

De Tommasi, G. et al. (2011). Current, position, and shape control in tokamaks. *Fusion Science and Technology*, 59(April (3)), 486–498.

De Tommasi, G., Ambrosino, G., Galeani, S., Maviglia, F., Neto, A. C., Pironti, A. et al. (2012). A software tool for the design of the current limit avoidance system at the JET tokamak. *IEEE Transactions on Plasma Science*, 40(August (8)), 2056–2064.

De Tommasi, G., Maviglia, F., Neto, A. C., Lomas, P. J., McCullen, P., Rimini, F. G. et al. (2014). Plasma position and current control system enhancements for the JET ITER-like wall. *Fusion Engineering and Design*, 89(March), 233–242.

De Tommasi, G. et al. (2014). Shape control with the eXtreme Shape Controller during plasma current ramp-up and ramp-down at JET tokamak. *Journal of Fusion Energy*, 33(March (2)), 233–242.

De Tommasi, G., Neto, A. C., Pironti, A., & Sterle, C. (2015). Optimal allocation of the diagnostic signals for the ITER magnetic control system. In *Proceedings of the 2015 IEEE multi-conference on systems and control* (pp. 1296–1302), Sydney, Australia, September.

Giruzzi, G., Joffrin E., Garcia J., Douai D., Artaud J.-F., Pégourié B., et al. (2016). Physics and operation oriented activities in preparation of the JT-60SA tokamak exploitation. In *Proceedings of the 26th IAEA fusion energy conference*, Kyoto, Japan, October.

Innocente, P., Barbato, P., Farthing, J., Giruzzi, G., Ide, S., Imbeaux, F. et al. (2015). Requirements for tokamak remote operation: Application to JT-60SA. *Fusion Engineering and Design*, 96–97, 799–802.

JT-60SA Research Unit. *JT-60SA Research Plan – Research Objectives and Strategy*. Technical report ⟨http://www.jt60sa.org/pdfs/JT-60SA_Res_Plan.pdf⟩.

JT-60SA Team (2015). *Plant integration document*. Technical report ⟨https://users.jt60sa.org/?uid=222UJY⟩.

Marchiori, G. et al. (2016). Design and operation of the RFX-mod plasma shape control system. *Fusion Engineering and Design*, 108(October), 81–91.

Miyata, Y., Suzuki, T., Ide, S., & Urano, H. (2014). Study of plasma equilibrium control for JT-60SA using MECS. *Plasma and Fusion Research*, 9 3403045-5.

Neto, A. C., Arshad, S., Sartori, F., Vayakis, G., Ambrosino, G., Batista, A. et al. (2015). Conceptual architecture of the plant system controller for the magnetics diagnostic of the ITER tokamak. *Fusion Engineering and Design*, 96–97(October), 887–890.

Pajares, A., & Schuster, E. (2016). Nonlinear burn control in tokamaks using in-vessel coils. In *Proceedings of the 2016 IEEE multi-conference on systems and control* (pp. 617–622), Buenos Aires, Argentina, September.

Peruzzo, S., Albanese, R., Artaserse, G., Coccorese, V., Gerasimov, S., Lam, N. et al. (2009). Installation and commissioning of the JET-EP magnetic diagnostic system. *Fusion Engineering and Design*, 84(June), 1495–1498.

Pironti, A., & Portone, A. (1998). Optimal choice of the geometrical descriptors for tokamak plasma shape control. *Fusion Engineering and Design*, 43(December (2)), 115–127.

Portone, A., Villone, F., Liu, Y., Albanese, R., & Rubinacci, G. (2008). Linearly perturbed MHD equilibria and 3D eddy current coupling via the control surface method. *Plasma Physics and Controlled Fusion*, 50(August (8)) 085004-12.

Romanelli, M., Corrigan, G., Parail, V., Wiesen, S., Ambrosino, R., Belo, P. et al. (2014). JINTRAC: A system of codes for integrated simulation of tokamak scenarios. *Plasma and Fusion Research*, 9(special issue 2) 3403023-1–4.

Sartori, F., De Tommasi, G., & Piccolo, F. (2006). The joint European torus. *IEEE Control Systems Magazine*, 26(April (2)), 64–78.

Shinya, K. (2000). Equilibrium analysis of tokamak plasma. *Journal of Plasma and Fusion Research*, 76(May (5)), 479–488.

Shirai, H., Barabaschi, P., & Kamada, Y. (2016). Progress of JT-60SA Project: EU-JA joint efforts for assembly and fabrication of superconducting tokamak facilities and its research planning. *Fusion Engineering and Design*, 109, 1701–1708. http://dx.doi.org/10.1016/j.fusengdes.2015.10.026.

Spears, W. R. (2014). JT-60SA construction status. *IEEE Transactions on Plasma Science*, 42(March), 427–431.

Tsunematsu, T. (2009). Broader approach to fusion energy. *Fusion Engineering and Design*, 84, 122–124.

Villone, F., Vyas, P., Lister, J. B., & Albanese, R. (1997). Comparison of the CREATE-L plasma response model with TCV limited discharges. *Nuclear Fusion*, 37(October (10)), 1395–1410.

Wenninger, R., Arbeiter, F., Aubert, J., Aho-Mantila, L., Albanese, R., Ambrosino, R. et al. (2015). Advances in the physics basis for the European DEMO design. *Nuclear Fusion*, 55(June (6)) 063003-7.

Yuan, Q. P., Xiao, B. J., Luo, Z. P., Walker, M. L., Welander, A. S., Hyatt, A. et al. (2013). Plasma current, position and shape feedback control on EAST. *Nuclear Fusion*, 53(April (4)), 043009.

Zabeo, L., Ambrosino, G., Cavinato, M., Gribov, Y., Kavin, A., Lukash, V. et al. (2014). Overview of magnetic control in ITER. *Fusion Engineering and Design*, 89(May (5)), 553–557.